Structure of the band tails in amorphous selenium

Structure of the band tails in amorphous selenium

M L Benkhedir[1,3], M Brinza[1,4], G J Adriaenssens[1,5] and C Main[2]

[1] University of Leuven, Halfgeleiderfysica, Celestijnenlaan 200D, B-3001 Leuven, Belgium
[2] University of Dundee, Division of Electronic Engineering and Physics, Nethergate, Dundee DD1 4HN, UK

E-mail: guy.adri@fys.kuleuven.be

Abstract
Transient photocurrent measurements on evaporated a-Se layers indicate the presence of two sets of discrete traps in the band tail region. The shallower traps, at $E_V + 0.20$ eV and $E_C - 0.28$ eV, are found to be electrically neutral, while the deeper ones at $E_V + 0.38$ eV and $E_C - 0.53$ eV are related to the charged negative-U centres of a-Se. The density of the discrete traps is of the same order of magnitude as the disorder-induced background density in the valence and conduction band tails, preventing the characterization of the a-Se tail-state densities by a simple functional form.

1. Introduction

The general observation of exponential Urbach tails in the optical absorption spectrum of amorphous semiconductors and the frequent use of exponential density-of-states (DOS) distributions for modelling calculations have led to the widely held notion that the band tails in those materials exhibit an exponentially decreasing density of localized states in the band gap. While early experiments involving transient photocurrents in As$_2$Se$_3$ [1] or time-of-flight (TOF) transients in a-Si:H [2] were interpreted in terms of such exponential DOS, careful examination of the experimental evidence frequently reveals that distribution to be inappropriate for describing the data [3], or to be valid as a first-order approximation to the real tail-state distribution only [4].

In the chalcogenide glasses, the charged coordination defects that form the basis of the *negative-U* model for explaining the absence of an equilibrium electron spin resonance signal [5] may be considered as prime candidates for interfering with a disorder-induced exponential band tail. However, the extent to which that interference can be experimentally verified is still under debate for some of the glasses. For instance, Tanaka [6] reported that the localized gap states in a-As$_2$S$_3$ are dominated by homopolar As–As bonding,

to the point where no trace of any coordination defects can be seen in the optical spectra. In a-Se on the other hand, the presence of discrete defect levels in the band tail region has been part of the conventional wisdom [7], but the energy position as well as the prominence of those levels did become an issue in recent years [8–11]. In view of the increased use of a-Se for digital x-ray imaging [12, 13], the density and energy position of electron and hole traps—and their concomitant capture and release rates—play an especially important role and warrant detailed investigation. Indeed, while the effect of ghosting in flat panel x-ray imaging detectors based on a-Se has been ascribed to electron trapping in localized states near the middle of the band gap [14, 15], a full analysis of the transient currents that lead to that conclusion would have to involve the influence of shallower traps with varying capture probabilities.

2. Results

In this contribution, we make use of transient photoconductivity (TPC) measurements, acquired under a wide range of experimental conditions, to determine the location and relative importance of two distinct sets of traps in the a-Se band tails. Figure 1 shows a set of a-Se TPC curves obtained on a ~15 μm thick a-Se layer with interdigitated Au contacts. The gap between the electrodes was 31 μm wide, 200 V was applied across the gap, and a 440 nm light pulse of 5 ns duration from a nitrogen-laser-triggered dye cell was used for carrier generation.
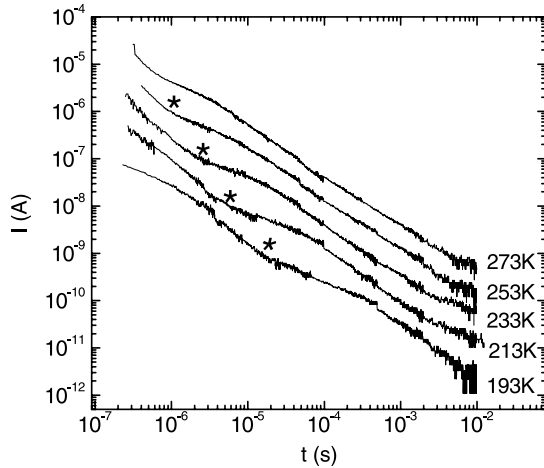
Figure 1. TPC signals from an a-Se layer at the indicated temperatures. The individual current traces are offset vertically for clarity. The asterisks point to the temperature-dependent position of the current dip.

Figure 2. Calculated $1/(I(t)t)$ plots based on the current data from figure 1. The arrows indicate choices for the time t^*.

Figure 3. a-Se DOS calculated from the current transients of figure 1 on the basis of a Fourier-transform-based formalism [21], using $\nu = 10^{12}$ s^{-1}. Individual curves have been offset vertically for clarity.

While for a purely exponential DOS, the trap-limited band transport mechanism, which controls the conductivity above 200 K in most amorphous semiconductors [16], would lead to a strictly power-law decay of the transient photocurrent after pulsed excitation, such behaviour is not observed for the TPC curves displayed in figure 1. Instead, a dip in the current transients is observed in the microsecond time range. Such a dip points to the presence of a discrete trapping level in the gap, with a density that exceeds the local background density [17–19]. Whenever—as is the case here—the dip is not very pronounced, i.e. when the density of the discrete level is of the order of the background density, the energy E_t of the trap with respect to the mobility edge can be deduced to good approximation from the relationship $t^* = \nu^{-1} \exp(E_t/kT)$, where the t^* is the time at the 'bottom' of the dip, ν is the attempt-to-escape frequency for the discrete trap, k the Boltzmann constant and T the temperature [18, 19]. By removing the downward slope from the measured TPC traces by converting them into $I(t)t$ or $1/(I(t)t)$ diagrams, the latter ones as shown in figure 2, appropriate t^* times can be readily obtained and used in a $\ln t^*$ versus $1/T$ plot to determine the approximate E_t and ν values of the trap. It may be noted that, for dispersive transport, such $1/(I(t)t)$ plots have been shown to provide a fair representation of the gap DOS [20].

Rather than the time-domain approximation described above for obtaining the trap position, it is possible—in principle—to obtain not just the trap position but an image of the surrounding DOS as well on the basis of a Fourier transform of the TPC curves [21]. Figure 3 presents the DOS profiles that are generated in this way, starting from the TPC traces of figure 1 and using an attempt-to-escape frequency $\nu = 10^{12}$ s^{-1}. The energy scale is defined by $E = kT \ln(\nu/\omega)$. As for figure 1, individual curves have been offset vertically for clarity. Apart from a more-or-less exponentially decreasing background, a distinct feature is seen near 0.3 eV at lower temperatures, and a broad shoulder manifests itself for higher energies at higher temperatures.
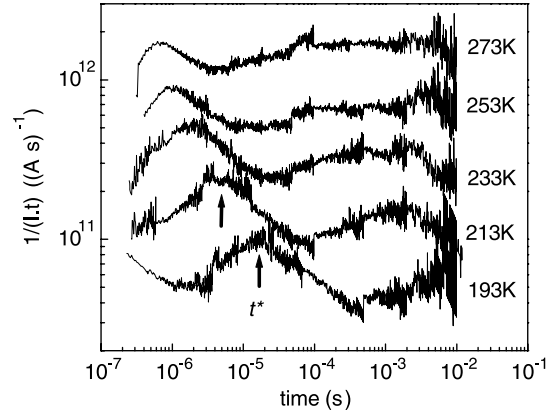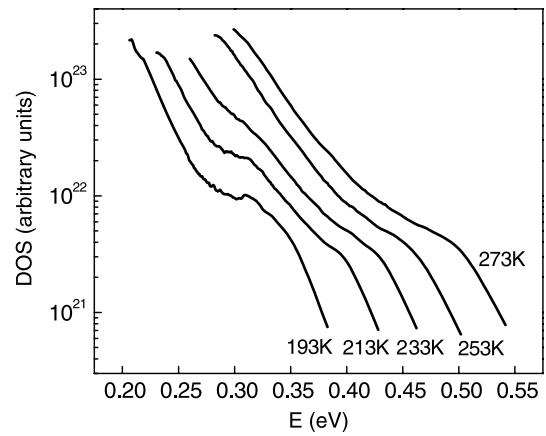
Given that holes are (by a factor of about 30) the more mobile charge carriers in a-Se, they will dominate the TPC signal. Features that are resolved from the current decay will hence correspond to elements of the DOS in the valence band tail. To obtain similar DOS information for the conduction band side of the gap, a photocurrent dominated by the electrons has to be generated. This can be achieved in the time-of-flight (TOF) experiment, whereby an a-Se layer is sandwiched between current-blocking contacts and a strongly absorbed light pulse creates free carriers just beyond one (semi-transparent) contact. An electric field across the sandwich cell will then, depending on its polarity, drift either electrons or holes through the cell and cause a matching conduction current in the external circuit. Up to the TOF transit time t_T, i.e. the time it takes for a representative set of the drifting carriers to reach the collection electrode, the transient current can be analysed with the same multiple-trapping model that is used for the TPC signals. Figure 4 shows a set of TOF transients obtained at different temperatures with a 16 μm thick a-Se sandwich cell under an applied voltage of 50 V. The slight dip in the pre-transit currents, recognizable from the slight changes
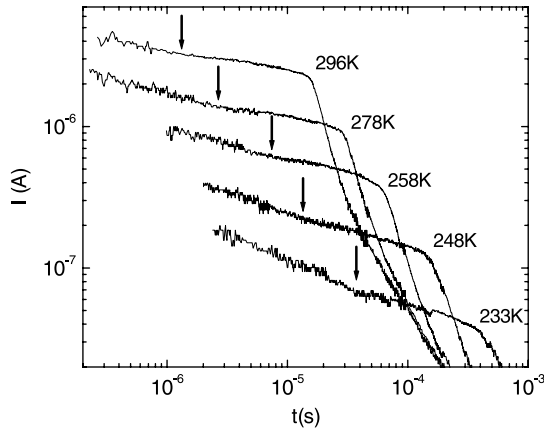
Figure 4. a-Se electron TOF transients measured at the indicated temperatures. The arrows point to the change of slope observed in the pre-transit currents.

of slope around the points indicated by the arrows in the figure, signals the presence of a shallow electron trap.

3. Discussion

Using the t^* values obtained from the traces in figure 2, and the $\ln t^* = \ln(1/\nu) + E_t/kT$ relationship suggested above, a shallow hole trap at approximately $E_{sh} = (0.20 \pm 0.02)$ eV above the valence band mobility edge and with an attempt frequency ν_{sh} in the range 5×10^8 s$^{-1} < \nu_{sh} < 2 \times 10^{10}$ s^{-1} can be resolved. A second data set, measured on a simple gap cell rather than an interdigitated structure, led to the values $E_{sh} = (0.18 \pm 0.03)$ eV and 2×10^8 s$^{-1} < \nu_{sh} < 2 \times 10^{10}$ s^{-1}. Apart from the indicated maximum at t^*, the figure 2 curves show further structure in the millisecond time range. That structure relates to one of the charged coordination defects of the negative-U model, as will be discussed below. As parameters for that defect we obtain $E_{Uh} = (0.38 \pm 0.02)$ eV and 2×10^{10} s$^{-1} < \nu_{Uh} < 1.3 \times 10^{12}$ s^{-1}.

The a-Se DOS profiles of figure 3 should ideally confirm and refine the defect parameters obtained from the time-domain analysis. As mentioned above, inspection of the figure 3 profiles indicates the presence of a DOS peak at ~0.31 eV from the lower-temperature curves and suggests a further broad feature around 0.45–0.50 eV in the DOS calculated from the highest-temperature data. These energy values are linked to the choice of $\nu = 10^{12}$ s^{-1} in the transform formalism through the $kT\ln(\nu/\omega)$ energy scale. In order to deduce the true E_t and ν values, one should be able to resolve the defect structure in a sequence of DOS profiles relating to TPC data obtained at different temperatures. By adjusting—if need be—the choice of ν in the calculation until a given feature is found at the same energy position for all temperatures, the defect's E_t and ν are found. Unfortunately, this procedure cannot be carried through for the results in figure 3 due to the limited time range of the TPC data, which restricts the available width of the DOS profile. In addition, those DOS profiles are distorted at both ends of the energy range due to that limited time window. In other words, we lack information

on the 0.45–0.50 eV feature at temperatures different from 273 K, and on the 0.31 eV peak at the higher temperatures. Nevertheless, shifting the 0.31 eV peak of the 193 K curve from its $\nu = 10^{12}$ s^{-1} position to the $\nu \approx 4 \times 10^9$ s^{-1} suggested by the time-domain analysis, we obtain a 0.22 eV position that agrees well with the earlier 0.20 eV value. Similarly, when moved to a $\nu \approx 2 \times 10^{11}$ s^{-1} position, the 0.45–0.50 eV structure of the 273 K curve moves down to ~0.41–0.46 eV which is close to the time domain 0.38 eV value.

The energy position of the defect near 0.4 eV corresponds to the energy of the negatively charged coordination defect (D^-) of the negative-U model for a-Se as determined earlier from an analysis of post-transit TOF currents and from the temperature dependence of the steady-state photocurrent [8]. The published post-transit TOF result of $E_{Uh} = (0.42 \pm 0.02)$ eV [22] is based on an assumed value of $\nu = 10^{12}$ s^{-1} and can therefore be compared to the 0.45–0.50 eV above. From the steady-state results, a D^- position of (0.36 ± 0.06) eV was deduced [23]. By applying the post-transit analysis to TOF transients obtained with varying values of the applied field, a systematic shift was observed of the E_{Uh} value towards the band edge, proportional to the square root of the field [22]. This phenomenon is known as the Poole–Frenkel effect and it indicates the charged character of those traps. No similar field dependence was observed in the TPC signals for the position of the shallow hole trap. The difference in attempt frequencies, around 4×10^9 s^{-1} for the shallow hole and electron traps and some 2×10^{11} s^{-1} for the negative-U centre, agrees with the different charge state of those defects. Indeed, charged centres will have larger capture cross sections and therefore, through the required detailed balance in equilibrium, correspondingly larger attempt-to-escape frequencies.

For the shallow defect near the conduction band mobility edge, the inflection points in the pre-transit currents shown in figure 4 lead to the parameters $E_{se} = (0.28 \pm 0.02)$ eV and 8×10^9 s$^{-1} < \nu_{se} < 6 \times 10^{10}$ s^{-1}. This value agrees with the ~0.30 eV obtained for this trapping level by Koughia *et al* [9] on the basis of numerical simulations of the electron TOF signals. It is not feasible, under the constraints of the TOF experiment, to increase the sample thickness to the point where the electron pre-transit current might show evidence for the anticipated negative-U D^+ centre on the conduction band side of the gap. However, the analysis of the *post-transit* part of the TOF signal makes it possible to position that centre at $E_{Ue} \cong 0.53$ eV below the mobility edge [8]. Here as well, a Poole–Frenkel shift of the E_{Ue} position was observed, while no such shift is detected for the inflection points in the pre-transit currents. In other words, the shallow level on the conduction band side of the gap also corresponds to a neutral defect, with the deeper negative-U centre obviously being charged.

Fourier-transform-based DOS curves for the conduction band tail were calculated on the basis of the TOF transients of figure 4. The curve based on the 296 K TOF data is displayed in figure 5. As with the hole-side DOS sections in figure 3, we find evidence for a deep centre at the high-energy end of the curve, i.e. at ~0.5 eV, but as before this signature is disturbed by the end-of-range distortion. The oscillatory pattern at the low-energy side of the DOS reflects the combined
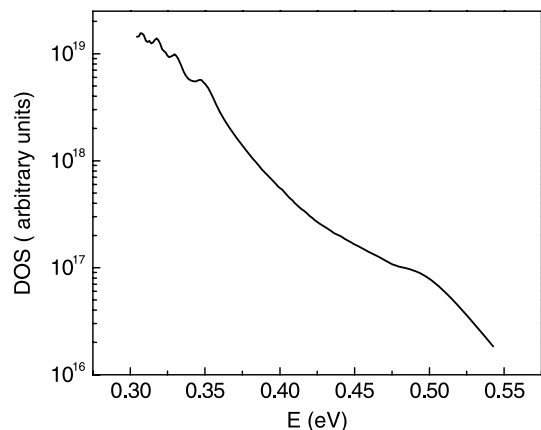
Figure 5. Fourier-transform-generated DOS based on the 296 K electron TOF transient (using $\nu = 10^{12}$ s^{-1}).

effect of the shallow defect and the abrupt current drop at the TOF transit time. That pattern moves as a unit with changing temperatures under the transforms with $\nu = 10^{12}$ s^{-1}, and can be made approximately temperature-independent and centred around 0.29 eV when $\nu \approx 8 \times 10^{10}$ s^{-1} is used.

The above results, either directly in the time domain or after transformation into the energy domain, indicate a remarkably symmetric defect structure superimposed on the valence and conduction band tail states of a-Se. The deeper levels at some 0.4–0.5 eV from the band edges have been identified before with the thermally accessible energy levels of the negative-U coordination defects [8, 23]. Due to their charged nature, they dominate the recombination in photoconductivity experiments, to the extent that their energy location also can be deduced from the thermal activation of steady-state photocurrents [23], in addition to the transient methods described above. The energy positions in the band gap of the E_{Uh} and E_{Ue} defect levels are in general agreement with the energies that are expected for them, some quarter of the band gap away from the band edges, on the basis of the theoretical negative-U models proposed for a-Se itself [24] or for the chalcogenide semiconductors in general [5, 25]. A similar agreement exists between the energy positions of the E_{sh} and E_{se} levels, around 0.2–0.3 eV removed from the band edges, and the predictions of a structural model that focuses on the dihedral angle between neighbouring Se lone-pair orbitals [26]. That model ascribes the appearance of intrinsic shallow defect states to the parallel rather than perpendicular alignment of neighbouring lone-pair orbitals. Such structural defects would of course be electrically neutral, as are the E_{sh} and E_{se} levels resolved from the TPC and electron TOF data.

4. Conclusions

Detailed investigations of transient photocurrents in a-Se films, be they TPC signals in gap cells or TOF results from sandwich cells, have shown that discrete defect-related energy bands constitute part of the electronic density of states in both conduction band and valence band tails. Their presence clearly contradicts the often-assumed exponentially varying tail-state density for a-Se. Those defects reduce any characterization of the observed disorder-related background density in terms of a specific functional form to the level of a rough approximation.

Acknowledgment

References

[1] Monroe D and Kastner M A 1986 *Phys. Rev.* B **33** 8881
[2] Street R A 1991 *Hydrogenated Amorphous Silicon* (Cambridge: Cambridge University Press)
[3] Marshall J M 1983 *Rep. Prog. Phys.* **46** 1235
[4] Brinza M, Emelianova E V and Adriaenssens G J 2005 *Phys. Rev.* B **71** 115209
[5] Street R A and Mott N F 1975 *Phys. Rev. Lett.* **35** 1293
[6] Tanaka K 2001 *J. Optoelectron. Adv. Mater.* **3** 189
[7] Abkowitz M 1988 *Phil. Mag. Lett.* **58** 53
[8] Benkhedir M L, Brinza M and Adriaenssens G J 2004 *J. Phys.: Condens. Matter* **16** S5253
[9] Koughia K, Shakoor Z, Kasap S O and Marshall J M 2005 *J. Appl. Phys.* **97** 033706
[10] Koughia K and Kasap S O 2006 *J. Non-Cryst. Solids* **352** 1539
[11] Emelianova E V, Benkhedir M L, Brinza M and Adriaenssens G J 2006 *J. Appl. Phys.* **99** 083702
[12] Kasap S O, Kabir M Z and Rowlands J A 2006 *Curr. Appl. Phys.* **6** 288
[13] Hoheisel M, Batz L, Mertelmeier T, Giersch J and Korn A 2006 *IEEE Trans. Nucl. Sci.* **53** 1118
[14] Zhao W, DeCrescenzo G, Kasap S O and Rowlands J A 2005 *Med. Phys.* **32** 488
[15] Bakueva L, Rau A W, Rowlands J A and Shik A 2006 *J. Phys. D: Appl. Phys.* **39** 441
[16] Monroe D 1985 *Phys. Rev. Lett.* **54** 146
[17] Marshall J M and Street R A 1984 *Solid State Commun.* **50** 91
[18] Seynhaeve G, Adriaenssens G J and Michiel H 1985 *Solid State Commun.* **56** 323
[19] Monroe D 1986 *Solid State Commun.* **60** 435
[20] Marshall J M 1985 *J. Non-Cryst. Solids* **77** 425
[21] Main C, Brüggeman R, Webb D P and Reynolds S 1993 *J. Non-Cryst. Solids* **164** 481
[22] Benkhedir M L, Aida M S and Adriaenssens G J 2004 *J. Non-Cryst. Solids* **344** 193
[23] Qamhieh N, Benkhedir M, Brinza M, Willekens J and Adriaenssens G J 2004 *J. Phys.: Condens. Matter* **16** 3827
[24] Kastner M, Adler D and Fritzsche H 1976 *Phys. Rev. Lett.* **37** 1504
[25] Karpov V G 1983 *Sov. Phys.—JETP* **58** 592
[26] Wong C K, Lucovsky G and Bernholc J 1987 *J. Non-Cryst. Solids* **97** 1171